Outflow boundary conditions for the lattice Boltzmann method

Michael Junk* and Zhaoxia Yang

FB Mathematik und Statistik, Universität Konstanz,
Postfach D194, 78457 Konstanz, Germany
E-mail: Michael.Junk@uni-konstanz.de
E-mail: Zhaoxia.Yang@uni-konstanz.de
*Corresponding author

Abstract: In this paper, we propose lattice Boltzmann implementations of several Navier-Stokes outflow boundary conditions like the zero normal-stress, the Neumann, and the do-nothing rule. A consistency analysis using asymptotic methods is given and the algorithms are numerically tested in two space dimensions with respect to accuracy and interaction with the inner flow field.

Keywords: lattice Boltzmann method; asymptotic analysis; outflow condition.

Biographical notes: Michael Junk received the doctoral degree (Dr. rer. nat.) in Mathematics from the University of Kaiserslautern, Germany, in 1997. Currently, he holds the Chair of Scientific Computing at the University of Constance, Germany. In 2003–2004, he was Professor for Numerics at the University of Saarbruecken. His research group focuses on various aspects of applied mathematics including the construction of mathematical models, their analysis and numerical solution. Since 1998, the analysis of lattice Boltzmann methods is one of the research topics.

Zhaoxia Yang received the first MSc in Applied Mathematics from Beijing University of Aeronautics and Astronautics, China, in 1994, the second master in Industrial Mathematics from the University of Kaiserslautern, Germany, in 2001, and the doctoral degree (Dr. rer. nat.) in Mathematics from the University of Constance, Germany, in 2007. From 2001, her research focus is lattice Boltzmann boundary conditions supported by DFG. She is currently a research member in the group of Professor M. Junk.

1 Lattice Boltzmann method

After almost two decades of research (Bhatnagar et al., 1954; Chen et al., 1991, 1992; Frisch et al., 1987; McNamara and Zanetti, 1988; Qian et al., 1992), the lattice Boltzmann method has become an interesting alternative for simulating incompressible flows. Nevertheless, lattice Boltzmann implementations of some conventional Navier-Stokes outflow conditions are rarely addressed or not available at all. This is the motivation for the considerations in this paper.

We present algorithms that are applicable for outflow boundaries which are orthogonal to a coordinate axis. This is perfectly suited for flows in axis parallel channels. But even curved and tilted channels can be covered under this geometrical restriction if the outflow boundary is not required to be orthogonal to the channel which may be the case whenever the outflow is artificial, i.e., only needed to simulate longer channels with less numerical effort.

The basic idea of the lattice Boltzmann method is to approximate the fluid velocity and pressure using a mesoscopic description based on particle movements obeying a kinetic equation. In order to set up the method, we cover the computational domain $\Omega \subset \mathbb{R}^d$ by a regular cubic lattice $h\mathbb{Z}^d$. The time domain $[0, T]$ is covered by a regular temporal grid with nodes $t_n = n\triangle t$. As relation between space and time step, we assume $\triangle t = h^2$ which reflects the diffusive time scaling necessary to recover the incompressible Navier-Stokes equation from Boltzmann-type equations (for further details, see Junk et al., 2005).

On this grid, the lattice Boltzmann evolution has the general form

$$f_i(n+1, \boldsymbol{j} + \boldsymbol{c}_i) = f_i(n, \boldsymbol{j}) + J_i(\boldsymbol{f}(n, \boldsymbol{j})), \qquad (1)$$

where $\mathbb{V} = \{\boldsymbol{c}_1, \dots, \boldsymbol{c}_N\} \subset \mathbb{R}^d$ is a discrete velocity set which possesses the symmetry property $\mathbb{V} = -\mathbb{V}$ and which is compatible with the spatial lattice $h\mathbb{Z}^d$ in the sense

that $\boldsymbol{j} + \boldsymbol{c}_i \in \mathbb{Z}^d$ for every $\boldsymbol{j} \in \mathbb{Z}^d$ and every $\boldsymbol{c}_i \in \mathbb{V}$. The evolution (1) is often split into a collision step

$$f_i^c(n, \boldsymbol{j}) = f_i(n, \boldsymbol{j}) + J_i(\boldsymbol{f}(n, \boldsymbol{j})),$$

followed by the transport step

$$f_i(n+1, \boldsymbol{j} + \boldsymbol{c}_i) = f_i^c(n, \boldsymbol{j}).$$

Apart from the general assumptions on the velocity set, we need some more structure for the implementation of our boundary conditions. In fact, the normal direction to the outflow boundary should also be a discrete velocity direction which leads to the requirement that $\mathbb{V}$ should contain all the axis directions $\mathbb{C} = \{\boldsymbol{e}_1, \ldots, \boldsymbol{e}_d\}$, i.e., there should be discrete velocities $\boldsymbol{c}_{m_k} = \|\boldsymbol{c}_{m_k}\|\boldsymbol{e}_k$ for all $k = 1, \ldots, d$. Moreover, for ease of presentation, we require that all velocity components $c_{ik} = \boldsymbol{c}_i \cdot \boldsymbol{e}_k$ are contained in $\{-1, 0, 1\}$. These extra assumptions are satisfied by many velocity models like D2Q9, D3Q15, D3Q19, and D3Q27.

The components $f_i(n, \boldsymbol{j})$ of the vector $\boldsymbol{f}(n, \boldsymbol{j})$ in (1) represent the density distributions of particles which are moving with velocity $\boldsymbol{c}_i$ at time level $t_n = nh^2$ and node $\boldsymbol{x}_{\boldsymbol{j}} = h\boldsymbol{j}$. The collision operator J is chosen to be of general relaxation type

$$J(\boldsymbol{f}) = A(\boldsymbol{f}^{eq}(\boldsymbol{f}) - \boldsymbol{f}), \tag{2}$$

and falls into the class of MRT models (see d'Humières et al., 2002). More specifically, we assume that the equilibrium distribution $\boldsymbol{f}^{eq}$ depends on $\boldsymbol{f}$ through the total mass density $\hat{\rho} = \sum_{i=1}^N f_i$ and the average velocity $\hat{\boldsymbol{u}} = \sum_{i=1}^N \boldsymbol{c}_i f_i$ according to

$$\boldsymbol{f}^{(eq)}(\boldsymbol{f}) = \boldsymbol{F}^{eq}(\hat{\rho}, \hat{\boldsymbol{u}}),$$
$$F_i^{eq}(\hat{\rho}, \hat{\boldsymbol{u}}) = f_i^*\left(\hat{\rho} + 3\hat{\boldsymbol{u}} \cdot \boldsymbol{c}_i + \frac{9}{2}\left((\hat{\boldsymbol{u}} \cdot \boldsymbol{c}_i)^2 - \frac{1}{3}|\hat{\boldsymbol{u}}|^2\right)\right).$$

Here $f_i^* = F_i^{eq}(1, 0)$ is a constant equilibrium obeying the symmetry property $f_i^* = f_{i^*}^*$ where i^* is the index of the velocity vector $\boldsymbol{c}_{i^*} = -\boldsymbol{c}_i$, and

$$\sum_{i=1}^N f_i^* = 1, \quad \sum_{i=1}^N c_{i\alpha}c_{i\beta}f_i^* = \frac{1}{3}\delta_{\alpha\beta},$$
$$\sum_{i=1}^N c_{i\alpha}c_{i\beta}c_{i\gamma}c_{i\delta}f_i^* = \frac{1}{9}(\delta_{\alpha\beta}\delta_{\gamma\delta} + \delta_{\alpha\delta}\delta_{\beta\gamma} + \delta_{\alpha\gamma}\delta_{\beta\delta}).$$

Note that the standard D2Q9, D3Q15, D3Q19, and D3Q27 weights fall into this class (Mei et al., 1999; Qian et al., 1992). It is stressed that only these models will be considered in this work.

The matrix $A \in \mathbb{R}^{N \times N}$ in (2) is a symmetric and positive semi-definite matrix with kernel generated by $\{\boldsymbol{1}, \boldsymbol{v}_1, \ldots, \boldsymbol{v}_d\}$. The components of the vector $\boldsymbol{1} \in \mathbb{R}^N$ are all 1 and $\boldsymbol{v}_\alpha \in \mathbb{R}^N$ is a vector with components $(c_{i\alpha})_{i=1,\ldots,N}$. Further we require that for every $\alpha, \beta \in \{1, \ldots, d\}$ the vectors $\boldsymbol{\Lambda}_{\alpha\beta}\boldsymbol{f}^*$ with components

$$(\boldsymbol{\Lambda}_{\alpha\beta}\boldsymbol{f}^*)_i = \left(c_{i\alpha}c_{i\beta} - \frac{1}{d}|\boldsymbol{c}_i|^2\right)f_i^*, \quad i = 1, \ldots, N$$

are eigenvectors of the collision matrix A with eigenvalue $1/(3\mu)$, i.e.,

$$A\boldsymbol{\Lambda}_{\alpha\beta}\boldsymbol{f}^* = \frac{1}{3\mu}\boldsymbol{\Lambda}_{\alpha\beta}\boldsymbol{f}^*, \quad \alpha, \beta \in \{1, \ldots, d\}. \tag{3}$$

This establishes the link to the fluid viscosity ν in form of $\nu = \mu - 1/6$. It is remarked that the well-known single relaxation time BGK model (dating back to Bhatnagar et al., 1954) can be subsumed in this approach by choosing $A = \frac{1}{\tau}P$ where P is the projection on the orthogonal complement of $\{\boldsymbol{1}, \boldsymbol{v}_1, \ldots, \boldsymbol{v}_d\}$. Since this projection is already realised by forming the difference $\boldsymbol{f}^{eq}(\boldsymbol{f}) - \boldsymbol{f}$, the projection P can be dropped, giving rise to the usual BGK operator $\frac{1}{\tau}(\boldsymbol{f}^{eq}(\boldsymbol{f}) - \boldsymbol{f})$ (more details are given in Junk et al., 2005). On a formal level, it seems that A is simply replaced by $\frac{1}{\tau}I$ as mentioned in Qian et al. (1992).

Assuming a proper initialisation (see Junk et al., 2005), both Chapman-Enskog expansion (Benzi et al., 1992; Chen et al., 1992; Chen and Doolen, 1998; d'Humières, 1992; Frisch et al., 1987; He and Luo, 1997a, 1997b) and asymptotic analysis (Junk and Yang, 2005; Junk et al., 2005) show that this lattice Boltzmann scheme is a second order accurate method for solving incompressible flows governed by the Navier-Stokes equation

$$\boldsymbol{\nabla} \cdot \boldsymbol{u} = 0, \quad \partial_t \boldsymbol{u} + (\boldsymbol{u} \cdot \nabla)\boldsymbol{u} + \nabla p = \nu\nabla^2\boldsymbol{u}, \quad \boldsymbol{u}|_{t=0} = \boldsymbol{\psi}. \tag{4}$$

Here, the velocity field $\boldsymbol{u}$ and the pressure field p are the unkowns. $\boldsymbol{\psi} : \Omega \to \mathbb{R}^d$ represents a divergence free initial velocity field.

2 Standard outflow conditions

When we consider flows in unbounded domains, e.g., flows in infinitely long channels, a difficulty arises because the computational domain has to be bounded so that an artificial open boundary is required at outflow. If the outflow condition is well-chosen, it is not necessary to deploy a very large computational domain in order to keep the essential part of the flow away from the influence of the outflow. Otherwise, unwanted effects of the outflow condition might propagate to the internal domain and lead to unrealistic results.

For flows governed by the Navier-Stokes system, much endeavor has been carried out in order to prescribe practically reasonable outflow conditions. Some of the most popularly applied outflow Boundary Conditions are listed here. The Neumann Boundary Condition (NBC) used, for example, in Abbassi et al. (2002),

$$\frac{\partial \boldsymbol{u}}{\partial \boldsymbol{n}}(t, \boldsymbol{x}) = \boldsymbol{\varphi}(t, \boldsymbol{x}), \quad \boldsymbol{x} \in \partial\Omega, \ t \in [0, T]; \tag{5}$$

or the Neumann-type "do-nothing condition (DNT)" from Heywood et al. (1996)

$$-p\boldsymbol{n} + \nu\frac{\partial \boldsymbol{u}}{\partial \boldsymbol{n}} = \boldsymbol{0}, \tag{6}$$

and the zero normal shear stress boundary condition (ZNS) or so-called no-friction condition (Ginzburg and Steiner, 2003; Mazya and Rossmann, 2006)

$$(-p\boldsymbol{I} + 2\nu S[\boldsymbol{u}])\boldsymbol{n} = 0, \quad S[\boldsymbol{u}] = \frac{1}{2}(\nabla\boldsymbol{u} + \nabla\boldsymbol{u}^T) \qquad (7)$$

are often suggested.

Another class of frequently used outflow condition are the so-called convective boundary conditions (see Ol'shanskii and Staroverov, 2000)

$$\frac{\partial\phi}{\partial t} + \bar{c}\frac{\partial\phi}{\partial \boldsymbol{n}} = 0$$

where ϕ can be some function of velocity, pressure or temperature, and $\bar{c}$ is a typical velocity.

The numerical realisation of these outflow conditions has been successfully demonstrated in Finite Difference (FD) and Finite Element Simulations (FEM) of Navier-Stokes equations.

However in lattice Boltzmann simulations, only the normal stress condition is addressed (see Ginzburg and Steiner, 2003, for example). Otherwise we encounter an extrapolation method in Yu et al. (2005) which operates directly on the distribution functions $\boldsymbol{f}$ and the treatment in Chikatamarla et al. (2006) which use Grad's approximation. None of the latter two treatments simulates one of the above mentioned conditions (see Section 3). In particular, the approximation of conditions (5) and (6) in the lattice Boltzmann context is still open.

In the following, we assume that the outflow boundary is chosen orthogonal to a coordinate axis with normal vector

$$\boldsymbol{n} = s\boldsymbol{e}_{k_0}, \quad s \in \{1, -1\}, \qquad (8)$$

where $\boldsymbol{e}_{k_0}$ is the k_0th unit axis vector. Then, we can rewrite the boundary conditions in a more explicit form. The NBC reads,

$$\frac{\partial\boldsymbol{u}}{\partial x_{k_0}}(t, \boldsymbol{x}) = s\boldsymbol{\varphi}(t, \boldsymbol{x}); \qquad (9)$$

DNT has the form

$$-p + \nu\frac{\partial u_{k_0}}{\partial x_{k_0}} = 0; \quad \nu\frac{\partial u_k}{\partial x_{k_0}} = 0, \ k \neq k_0; \qquad (10)$$

and ZNS can be written as

$$-p + 2\nu\frac{\partial u_{k_0}}{\partial x_{k_0}} = 0; \quad 2\nu S[\boldsymbol{u}] : \boldsymbol{e}_k \otimes \boldsymbol{e}_{k_0} = 0, \ k \neq k_0. \tag{11}$$

Here $\otimes$ is the symmetric tensor product among two vectors $\boldsymbol{a}$ and $\boldsymbol{b}$ and $: -$ is the product between two matrices A and B

$$(\boldsymbol{a} \otimes \boldsymbol{b})_{ij} = (a_i b_j + a_j b_i)/2, \quad A : B = \sum_{i,j=1}^{d} A_{ij} B_{ij}.$$

For the numerical treatment, we will assume that the grid nodes are located exactly on the outflow boundary.

3   Analysis of existing methods

We briefly analyse some existing outflow algorithms in order to see whether they approximate the conditions listed in the previous section.

While it is obvious from the construction of the free interface condition in Ginzburg and Steiner (2003) that it approximates a normal stress condition of a slightly more general type than (7) on general boundary geometries, the macroscopic behaviour of the methods presented in Chikatamarla et al. (2006) and Yu et al. (2005) is not so clear. In order to see whether the macroscopic behaviour matches a Neumann type condition, we use the asymptotic analysis presented in Junk and Yang (2005). This approach provides information about the whole algorithm including the boundary scheme order by order in h.

The idea is to approximate the lattice Boltzmann solution in terms of a regular expansion of the form

$$f_i(n, \boldsymbol{j}) = f_i^{(0)}(t_n, \boldsymbol{x}_j) + hf_i^{(1)}(t_n, \boldsymbol{x}_j) \\ + h^2 f_i^{(2)}(t_n, \boldsymbol{x}_j) + \cdots \qquad (12)$$

where $f_i^{(k)}(t, \boldsymbol{x})$ are smooth functions of time $t \in [0, T]$ and spatial variable $\boldsymbol{x} \in \Omega$. To fix the coefficients, we require that the expansion satisfies the lattice Boltzmann equation (1) as accurately as possible. To achieve this goal, we insert (12) into (1), perform a Taylor expansion and choose the coefficients such that the residue is of highest possible order in h. In this way, we find the coefficients. The first three are

$$f_i^{(0)} = f_i^*,$$
$$f_i^{(1)} = 3f_i^* \boldsymbol{c}_i \cdot \boldsymbol{u},$$
$$f_i^{(2)} = f_i^* \left[3p + \frac{9}{2}(\boldsymbol{c}_i \cdot \boldsymbol{u})^2 - \frac{3}{2}|\boldsymbol{u}|^2\right] - (A^\dagger(\mathbf{V} \cdot \nabla)\boldsymbol{f}^{(1)})_i.$$

For the other coefficients we refer to Junk and Yang (2005) and Junk et al. (2005). Here, $\boldsymbol{u}$ and p are solutions of the Navier-Stokes equation (4). $A^\dagger$ is the pseudo inverse of A and $(\mathbf{V} \cdot \nabla)^k \boldsymbol{f}$ abbreviates

$$(\mathbf{V} \cdot \nabla)^k \boldsymbol{f} = \left[(\boldsymbol{c}_1 \cdot \nabla)^k f_1, \dots, (\boldsymbol{c}_N \cdot \nabla)^k f_N\right]^T.$$

First we analyse the extrapolation treatment presented in Yu et al. (2005). If the normal $\boldsymbol{n}$ to the outflow boundary is parallel to one axis and $\boldsymbol{c}_i$ is an incoming direction at boundary node $\boldsymbol{x}_j$, this method reads

$$f_i(n+1, \boldsymbol{j}) = 2f_i(n+1, \boldsymbol{j} - \boldsymbol{n}) - f_i(n+1, \boldsymbol{j} - 2\boldsymbol{n}).$$

It is noted that $\boldsymbol{x_{j-n}}$ and $\boldsymbol{x_{j-2n}}$ are lattice nodes in Ω under the geometrical assumption on the outflow boundary. Inserting Equation (12) with coefficients up to $\boldsymbol{f}^{(3)}$ into the boundary condition, then doing Taylor expansion at $(t_n, \boldsymbol{x_j})$ and equating terms of the same order in h, we find the trivial condition $0 = 0$ in orders h^k ($k = 0, 1, 2$). The first non-trivial conditions appear in order h^3 and have the form $(\boldsymbol{n} \cdot \nabla)^2(\boldsymbol{u} \cdot \boldsymbol{c}_i) = 0$, where i denotes the indices of the incoming directions. In the geometrical case considered

here, we can find a maximal set of linearly independent directions among the incoming directions (Fig. 1 shows an example for the 2D case). Therefore the separate link-based conditions can be summarised in the form of a macroscopic boundary condition

$$(\boldsymbol{n} \cdot \nabla)^2 \boldsymbol{u} = 0$$

which involves *second* order derivatives of the velocity field and thus is not in the class of conditions presented in Section 2.

Figure 1 Left: Demonstration of the ghost node $\boldsymbol{x}_{j_0}$ to a boundary node $\boldsymbol{x}_j$. The vector $\boldsymbol{n}$ is the outward normal direction. Right: A part of the boundary Γ with a node $\boldsymbol{x}_j$ and three incoming directions
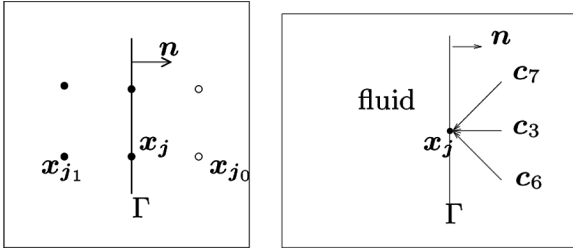
Next, let us investigate the method introduced in Chikatamarla et al. (2006), which reads

$$
\begin{aligned}
&f_i(n+1, \boldsymbol{j}) \\
&= f_i^*[\hat{\rho}(n, \boldsymbol{j}) + 3\boldsymbol{c}_i \cdot \hat{\boldsymbol{u}}(n, \boldsymbol{j})] \\
&\quad + f_i^*\left[\frac{9}{2}\left(\sum_k f_k(n, \boldsymbol{j})\boldsymbol{c}_k \otimes \boldsymbol{c}_k - \frac{1}{3}\hat{\rho}(n, \boldsymbol{j})\boldsymbol{I}\right) : \right. \\
&\quad\quad\left. \left(\boldsymbol{c}_i \otimes \boldsymbol{c}_i - \frac{1}{3}\boldsymbol{I}\right)\right].
\end{aligned}
\tag{13}
$$

Applying a similar procedure to Equation (13) as before, gives rise to the condition

$$
\begin{aligned}
\partial_t f_i^{(1)} - &\left(A^\dagger\left(\partial_t \boldsymbol{f}^{(1)} + (\mathbf{V} \cdot \nabla)\boldsymbol{f}^{(2)}\right.\right. \\
&\left.\left.+ \frac{1}{2}(\mathbf{V} \cdot \nabla)^2 \boldsymbol{f}^{(1)}\right)\right)_i = 0.
\end{aligned}
\tag{14}
$$

Using the explicit structure of the coefficients $\boldsymbol{f}^{(k)}$ and observing that there are enough linearly independent incoming directions, Equation (14) leads to an unusual condition on $\boldsymbol{u}$, again containing second order spatial derivatives. For example, in the LBGK D2Q9 case, we find

$$
\begin{aligned}
&\partial_t \boldsymbol{u} - \tau\left[\frac{2}{3}\nu\triangle\boldsymbol{u} - (\boldsymbol{u} \cdot \nabla)\boldsymbol{u} + \nabla(\|\boldsymbol{u}\|^2)\right. \\
&\left.- \frac{3}{2}\begin{pmatrix} \partial_x u_1 & -\partial_y u_1 \\ -\partial_x u_2 & \partial_y u_2 \end{pmatrix}\boldsymbol{u} + 2\left(\tau - \frac{1}{2}\right)\partial_{xy}\begin{pmatrix} u_2 \\ u_1 \end{pmatrix}\right] = 0
\end{aligned}
$$

where τ is the single relaxation parameter of the BGK model.

4 Lattice Boltzmann algorithms

4.1 Neumann Boundary Condition (NBC)

For a prescribed Neumann boundary condition (5), a practical second order accurate realisation in finite difference methods is obtained by introducing so-called ghost nodes for each boundary node, such that the pairs of ghost and boundary nodes are symmetric with respect to the boundary $\partial\Omega$. For example, Figure 1 shows a 2D case where $\boldsymbol{x}_{j_1} \in \Omega$ is a fluid node next to the outflow boundary node $\boldsymbol{x}_j$ on Γ and $\boldsymbol{x}_{j_0}$ is its ghost node. Observe that $\boldsymbol{x}_j$ is the intersection point of the boundary and the connecting line betweens $\boldsymbol{x}_{j_1}$ and $\boldsymbol{x}_{j_0}$.

The general idea is to assign the velocity value

$$\boldsymbol{\phi}(t, \boldsymbol{x}_{j_0}) = \boldsymbol{u}(t, \boldsymbol{x}_{j_1}) + 2h\boldsymbol{\varphi}(t, \boldsymbol{x}_j)$$

at the ghost node, i.e.,

$$\boldsymbol{u}(t, \boldsymbol{x}_{j_0}) = \boldsymbol{\phi}(t, \boldsymbol{x}_{j_0}), \tag{15}$$

so that

$$
\begin{aligned}
\frac{\partial \boldsymbol{u}}{\partial \boldsymbol{n}}(t, \boldsymbol{x}_j) &= \frac{\boldsymbol{u}(t, \boldsymbol{x}_{j_0}) - \boldsymbol{u}(t, \boldsymbol{x}_{j_1})}{2h} + \mathcal{O}(h^2) \\
&= \boldsymbol{\varphi}(t, \boldsymbol{x}_j) + \mathcal{O}(h^2),
\end{aligned}
$$

and a second order accurate Neumann boundary condition is achieved.

To realise the Dirichlet condition (15) in the lattice Boltzmann setup, we apply the BFL method from Bouzidi et al. (2001). Noting that the LB average velocity $\hat{\boldsymbol{u}}(n, \boldsymbol{j})$ is an approximation of the scaled Navier-Stokes solution $h\boldsymbol{u}(t_n, \boldsymbol{x}_j)$, we use the Dirichlet boundary values

$$\hat{\phi}(n, j_0) = \frac{1}{h}\hat{\boldsymbol{u}}(n, \boldsymbol{j}_1) + 2h\boldsymbol{\varphi}(t_n, \boldsymbol{x}_j)$$

Then, if $\boldsymbol{c}_i$ is an incoming direction at ghost node $\boldsymbol{x}_{j_0}$, the BFL scheme to obtain the boundary value $\hat{\phi}$ has the form

$$
\begin{aligned}
f_i(n+1, \boldsymbol{j}_0) &= f_{i^*}^c(n, \boldsymbol{j}_0 + \boldsymbol{c}_i) \\
&\quad + 6f_i^* h\, \hat{\phi}(n, \boldsymbol{j}_0) \cdot \boldsymbol{c}_i.
\end{aligned}
\tag{16}
$$

Asymptotic analysis. The analysis is started by inserting the expansion (12) (using the second order approximation below (12)) into (16) and applying a Taylor expansion around $(t, \boldsymbol{x}_{ji})$ which is the intersection on the boundary Γ along the link in the direction of $\boldsymbol{c}_i$. In fact $\boldsymbol{x}_{ji} = \boldsymbol{x}_{j_0} + h\boldsymbol{c}_i$ and $\boldsymbol{x}_{ji} = \boldsymbol{x}_j + h(\boldsymbol{c}_i + \boldsymbol{n})$. After a straight forward calculation and cancelling out all the possible terms we are left with

$$6h^2\left(\frac{\partial \boldsymbol{u}}{\partial \boldsymbol{n}} - \boldsymbol{\varphi}\right) \cdot \boldsymbol{c}_i f_i^* + \mathcal{O}(h^3) = 0. \tag{17}$$

This demonstrates the accuracy of at least first order for the Neumann boundary condition.

4.2 Zero normal shear stress boundary (ZNS)

From the asymptotic analysis in Junk and Yang (2005), we know

$$f_i = F_i^{eq}(\hat{\rho}, \hat{\boldsymbol{u}}) - h^2 (A^\dagger (\mathbf{V} \cdot \nabla) \boldsymbol{f}^{(1)})_i + \mathcal{O}(h^3). \qquad (18)$$

Substituting the formula of $\boldsymbol{f}^{(1)}$ and using the notation $\mathbf{V} \otimes \mathbf{V} \boldsymbol{f}^* : S[\boldsymbol{u}]$ to denote the vector

$$(\mathbf{V} \otimes \mathbf{V} \boldsymbol{f}^* : S[\boldsymbol{u}])_i = \sum_{\alpha,\beta} f_i^* \boldsymbol{c}_{i\alpha} \boldsymbol{c}_{i\beta} S_{\alpha\beta}[\boldsymbol{u}],$$

we have

$$f_i = F_i^{eq}(\hat{\rho}, \hat{\boldsymbol{u}}) - h^2 (3A^\dagger \mathbf{V} \otimes \mathbf{V} \boldsymbol{f}^* : S[\boldsymbol{u}])_i + \mathcal{O}(h^3) \quad (19)$$

which shows how the viscous stresses enter into the expansion of the distribution functions. Further using $\hat{\rho} = 1 + 3h^2 p + \mathcal{O}(h^3)$, we obtain

$$f_i = F_i^{eq}(1, \hat{\boldsymbol{u}}) + 3h^2 p f_i^* - 3h^2$$
$$\times (A^\dagger \mathbf{V} \otimes \mathbf{V} \boldsymbol{f}^* : S[\boldsymbol{u}])_i + \mathcal{O}(h^3). \qquad (20)$$

Again from the asymptotic analysis in Junk and Yang (2005), it follows that

$$h^2 3\mathbf{V} \otimes \mathbf{V} \boldsymbol{f}^* : S[\boldsymbol{u}] = -A(\boldsymbol{f} - \boldsymbol{f}^{eq}) + \mathcal{O}(h^3). \qquad (21)$$

Our aim is to construct an implementation of the zero normal shear stress boundary condition with the help of these formulas.

The required structure of the velocity set in connection with the assumption that the outflow surface is perpendicular to an axis direction guarantees that one of the incoming directions, say $\boldsymbol{c}_{k_0}$, must be opposite to the outer normal direction $\boldsymbol{n}$. The proposed implementation treats this direction differently from the other incoming directions. Note that, for $\boldsymbol{c}_{k_0} = -\boldsymbol{c}_{k_0^*}$,

$$\boldsymbol{c}_{k_0^*} \otimes \boldsymbol{c}_{k_0^*} = \boldsymbol{c}_{k_0} \otimes \boldsymbol{c}_{k_0} = \boldsymbol{n} \otimes \boldsymbol{n}, \quad S[\boldsymbol{u}] : \boldsymbol{n} \otimes \boldsymbol{n} = \frac{\partial u_{k_0}}{\partial x_{k_0}}. \qquad (22)$$

Applying the first condition of (11), we can replace the pressure term in (20) using Equations (21) and (22),

$$3h^2 p f_{k_0}^* = 6h^2 \nu f_{k_0^*}^* S[\boldsymbol{u}] : \boldsymbol{c}_{k_0^*} \otimes \boldsymbol{c}_{k_0^*}$$
$$= -2\nu (A(\boldsymbol{f} - \boldsymbol{f}^{eq}))_{k_0^*} + \mathcal{O}(h^3). \qquad (23)$$

Altogether, Equation (20) turns into a condition for the distribution function along the incoming direction $\boldsymbol{c}_{k_0}$,

$$f_{k_0}(n+1, \boldsymbol{j}) = F_{k_0}^{eq}(1, \hat{\boldsymbol{u}}(n, \boldsymbol{j})) - ((2\nu A - \boldsymbol{I})(\boldsymbol{f}(n, \boldsymbol{j})$$
$$- \boldsymbol{f}^{eq}(n, \boldsymbol{j})))_{k_0^*}. \qquad (24)$$

Next, we want to introduce the other conditions of Equation (11). Using property (3) and $tr(S[\boldsymbol{u}]) = \nabla \cdot$

$\boldsymbol{u} = 0$, we first rewrite the term with $A^\dagger$ in Equations (19) and (20) by

$$3A^\dagger \mathbf{V} \otimes \mathbf{V} \boldsymbol{f}^* : S[\boldsymbol{u}] = 3A^\dagger \boldsymbol{\Lambda} \boldsymbol{f}^* : S[\boldsymbol{u}] = 9\mu \boldsymbol{\Lambda} \boldsymbol{f}^* : S[\boldsymbol{u}]$$
$$= 9\mu \mathbf{V} \otimes \mathbf{V} \boldsymbol{f}^* : S[\boldsymbol{u}] \qquad (25)$$

where $\boldsymbol{\Lambda} \boldsymbol{f}^* : S[\boldsymbol{u}]$ denotes the vector

$$(\boldsymbol{\Lambda} \boldsymbol{f}^* : S[\boldsymbol{u}])_i = \sum_{\alpha,\beta} f_i^* \Lambda_{i\alpha\beta} S_{\alpha\beta}[\boldsymbol{u}].$$

For the ith component, this implies

$$3(A^\dagger \mathbf{V} \otimes \mathbf{V} \boldsymbol{f}^* : S[\boldsymbol{u}])_i = 9\mu f_i^* \boldsymbol{c}_i \otimes \boldsymbol{c}_i : S[\boldsymbol{u}]. \qquad (26)$$

Next, we rewrite $\boldsymbol{c}_i \otimes \boldsymbol{c}_i$ in terms of the products $\boldsymbol{e}_k \otimes \boldsymbol{e}_{k_0}$ so that the stress conditions on $\boldsymbol{e}_k \otimes \boldsymbol{e}_{k_0} : S[\boldsymbol{u}]$ can be used.

If $\boldsymbol{c}_i$ is an incoming direction different from $\boldsymbol{c}_{k_0}$, we can express it in the form $\boldsymbol{c}_i = \sum_{k=1}^d c_{ik} \boldsymbol{e}_k$ with respect to the standard basis $\{\boldsymbol{e}_k\}$. In view of Equation (8), we can rewrite this relation in the form

$$\boldsymbol{c}_i = s c_{ik_0} \boldsymbol{n} + \sum_{k \neq k_0} c_{ik} \boldsymbol{e}_k.$$

Since $\boldsymbol{c}_i$ is incoming, we have $\boldsymbol{c}_i \cdot \boldsymbol{n} < 0$, i.e., $c_{ik_0} \neq 0$. Moreover, there must be an additional $c_{ik} \neq 0$ because $\boldsymbol{c}_i \neq \boldsymbol{c}_{k_0}$. Hence, we have

$$\boldsymbol{c}_i \otimes \boldsymbol{c}_i = \sum_{k=1}^d c_{ik}^2 \boldsymbol{e}_k \otimes \boldsymbol{e}_k + \sum_{k \neq k_0} c_{ik} c_{ik_0} \boldsymbol{e}_k \otimes \boldsymbol{e}_{k_0}$$
$$+ \sum_{\substack{k \neq l \\ k,l \neq k_0}} c_{ik} c_{il} \boldsymbol{e}_k \otimes \boldsymbol{e}_l. \qquad (27)$$

Using the stress conditions

$$\sum_{k=1}^d \boldsymbol{e}_k \otimes \boldsymbol{e}_k : S[\boldsymbol{u}] = \nabla \cdot \boldsymbol{u} = 0,$$

and

$$\sum_{k \neq k_0} c_{ik} \boldsymbol{e}_k \otimes \boldsymbol{e}_{k_0} : S[\boldsymbol{u}] = 0,$$

where the latter is a linear combination of the conditions in Equation (11), we find

$$\boldsymbol{c}_i \otimes \boldsymbol{c}_i : S[\boldsymbol{u}] = \sum_{k=1}^d (c_{ik}^2 - 1) \boldsymbol{e}_k \otimes \boldsymbol{e}_k : S[\boldsymbol{u}]$$
$$+ \sum_{\substack{k \neq l \\ k,l \neq k_0}} c_{ik} c_{il} \boldsymbol{e}_k \otimes \boldsymbol{e}_l : S[\boldsymbol{u}]. \qquad (28)$$

We continue by distinguishing two natural cases:

i   For incoming directions $\boldsymbol{c}_i$ with $c_{ik}^2 = 1$ for all k, like $(-1, 1)$ in the D2Q9 case or $(1, -1, 1)$ in the D3Q15 model, the first sum in Equation (28) drops out, so that

$$\boldsymbol{c}_i \otimes \boldsymbol{c}_i : S[\boldsymbol{u}] = \sum_{\substack{k \neq l \\ k,l \neq k_0}} c_{ik} c_{il} \boldsymbol{e}_k \otimes \boldsymbol{e}_l : S[\boldsymbol{u}]. \qquad (29)$$

Further since $e_k \otimes e_l : S[u]$ are off-diagonal terms in $S[u]$ they can be computed from suitable velocity averages of $f - f^{eq}$ (see details in Junk and Yang, 2005). In view of Equation (20) we set

$$
\begin{aligned}
f_i(n+1, \boldsymbol{j}) = {} & F_i^{eq}(1, \hat{\boldsymbol{u}}(n, \boldsymbol{j})) \\
& - \frac{f_i^*}{f_{k_0}^*}(2\nu A(\boldsymbol{f}(n, \boldsymbol{j}) - \boldsymbol{f}^{eq}(n, \boldsymbol{j})))_{k_0^*} \\
& + 9 \sum_{\substack{k \neq l \\ k, l \neq k_0}} c_{ik} c_{il} f_i^* \sum_{p=1}^{N} c_{pk} c_{pl} \\
& \times (\boldsymbol{f}_p(n, \boldsymbol{j}) - \boldsymbol{f}_p^{eq}(n, \boldsymbol{j}))
\end{aligned}
\tag{30}
$$

where the required pressure term is computed according to Equation (23).

ii   For the remaining incoming directions, e.g., $(1, -1, 0)$ in the D3Q19 model, at least one of the two non-normal components vanishes so that $c_{ik}c_{il} = 0$ for $k \neq l$ and $k, l \neq k_0$. Hence, Equation (28) implies

$$
\boldsymbol{c}_i \otimes \boldsymbol{c}_i : S[\boldsymbol{u}] = \sum_{k=1}^{d}(c_{ik}^2 - 1)\boldsymbol{e}_k \otimes \boldsymbol{e}_k : S[\boldsymbol{u}].
$$

Relation (19) then leads to the condition

$$
\begin{aligned}
f_i(n+1, \boldsymbol{j}) = {} & f_i^{eq}(n, \boldsymbol{j}) + \sum_{k=1}^{d}(c_{ik}^2 - 1)\frac{f_i^*}{f_{m_k}^* \|\boldsymbol{c}_{m_k}\|^2} \\
& \times (\boldsymbol{f}_{m_k}(n, \boldsymbol{j}) - \boldsymbol{f}_{m_k}^{eq}(n, \boldsymbol{j}))
\end{aligned}
\tag{31}
$$

where $\boldsymbol{c}_{m_k} = \|\boldsymbol{c}_{m_k}\|\boldsymbol{e}_k$ are the velocities pointing in the coordinate directions.

In summary, the zero-normal-stress condition consists of Equation (24) for the normal incoming direction and Equations (30) and (31) for the incoming directions covered by case (i) and (ii). We stress that for the D2Q9 and D3Q15 models, only case (i) appears. The D3Q19 model involves (ii) and D3Q27 requiress both (i) and (ii).

Asymptotic analysis. After a standard calculation following the routine procedure outlined in Section 3, Equation (24) turns into

$$
\begin{aligned}
& h^2 3 f_{k_0}^*(p - 2\nu(\boldsymbol{n} \cdot \nabla)(\boldsymbol{u} \cdot \boldsymbol{n})) \\
& - 2h^3 \nu \left(\partial_t f_{k_0}^{(1)} - (\boldsymbol{c}_{k_0} \cdot \nabla) f_{k_0}^{(2)} + \frac{1}{2}(\boldsymbol{c}_{k_0} \cdot \nabla)^2 f_{k_0}^{(1)} \right) \\
& = \mathcal{O}(h^4)
\end{aligned}
\tag{32}
$$

The coefficient of h^2 in Equation (32) yields

$$
p - 2\nu(\boldsymbol{n} \cdot \nabla)(\boldsymbol{u} \cdot \boldsymbol{n}) = 0.
$$

This equation actually corresponds to the first equation in (11), noting that $\boldsymbol{n}$ is a constant coordinate direction. Processing of Equation (30) leads to

$$
\begin{aligned}
& h^2 \Bigg(3 f_i^*(p - 2\nu(\boldsymbol{n} \cdot \nabla)(\boldsymbol{u} \cdot \boldsymbol{n})) - 3(A^\dagger \boldsymbol{\Lambda} \boldsymbol{f}^* : S[\boldsymbol{u}])_i \\
& + 27 \sum_{\substack{k \neq l \\ k, l \neq k_0}} c_{ik} c_{il} f_i^* \sum_{p=1}^{N} c_{pk} c_{pl}(A^\dagger \boldsymbol{\Lambda} \boldsymbol{f}^* : S[\boldsymbol{u}])_p \Bigg) \\
& = \mathcal{O}(h^3).
\end{aligned}
\tag{33}
$$

Since the first term in the h^2 coefficient of Equation (33) vanishes, we are left with

$$
\begin{aligned}
& (A^\dagger \boldsymbol{\Lambda} \boldsymbol{f}^* : S[\boldsymbol{u}])_i \\
& - 9 \sum_{\substack{k \neq l \\ k, l \neq k_0}} c_{ik} c_{il} f_i^* \sum_{p=1}^{N} c_{pk} c_{pl}(A^\dagger \boldsymbol{\Lambda} \boldsymbol{f}^* : S[\boldsymbol{u}])_p = 0.
\end{aligned}
\tag{34}
$$

Using property (3), Equation (34) turns out to be

$$
\Lambda_i f_i^* : S[\boldsymbol{u}] - 9 \sum_{\substack{k \neq l \\ k, l \neq k_0}} c_{ik} c_{il} f_i^* \sum_{p=1}^{N} c_{pk} c_{pl} \Lambda_p f_p^* : S[\boldsymbol{u}] = 0.
$$

Taking into account $\nabla \cdot \boldsymbol{u} = 0$ and

$$
9 \sum_{p=1}^{N} c_{pk} c_{pl} \Lambda_p f_p^* : S[\boldsymbol{u}] = \boldsymbol{e}_k \otimes \boldsymbol{e}_l : S[\boldsymbol{u}],
$$

we get

$$
\boldsymbol{c}_i \otimes \boldsymbol{c}_i : S[\boldsymbol{u}] - \sum_{\substack{k \neq l \\ k, l \neq k_0}} c_{ik} c_{il} \boldsymbol{e}_k \otimes \boldsymbol{e}_l : S[\boldsymbol{u}] = 0.
\tag{35}
$$

Calculating $\boldsymbol{c}_i \otimes \boldsymbol{c}_i$ through Equation (27), we obtain from Equation (35)

$$
\sum_{k \neq k_0} c_{ik} \boldsymbol{e}_k \otimes \boldsymbol{e}_{k_0} : S[\boldsymbol{u}] = 0.
\tag{36}
$$

A similar process applied to Equation (31) leads to

$$
\boldsymbol{c}_i \otimes \boldsymbol{c}_i : S[\boldsymbol{u}] - \sum_{k=1}^{d}(c_{ik}^2 - 1)\boldsymbol{e}_k \otimes \boldsymbol{e}_k : S[\boldsymbol{u}] = 0.
$$

Noting that the last term on the right side of (27) disappears for the considered case (ii), we again obtain condition (36). Finally, our assumption on the structure of the velocity model guarantees that all tangential directions $\boldsymbol{e}_k, k \neq k_0$ appear. Hence, we successfully recover the second set of equations in (11).

Moreover the coefficient of h^3 in (32) is generally not zero so that the boundary scheme (24), (30) and (31) renders a first order accurate approximation of the zero normal stress condition (7).

4.3 Do-Nothing Condition (DNT)

To realise the do-nothing condition (10) in lattice Boltzmann simulations, we combine formula (24) and a straight forward extension of the Neumann boundary scheme (16). Again we use the condition that $\boldsymbol{n}$ is opposite to one of the incoming directions, say $\boldsymbol{n} = -\boldsymbol{c}_{k_0}$. Since the first equation in (10) differs only by a factor 2 from the one in (11), a similar strategy as in the previous section gives rise to the condition

$$
f_{k_0}(n+1, \boldsymbol{j}) = F_{k_0}^{eq}(1, \hat{\boldsymbol{u}}(n, \boldsymbol{j}))
$$
$$
- ((\nu A - \boldsymbol{I})(\boldsymbol{f}(n, \boldsymbol{j}) - \boldsymbol{f}^{eq}(n, \boldsymbol{j})))_{k_0^*}. \tag{37}
$$

The remaining equations in (10) appear as zero Neumann boundary conditions for the velocity components perpendicular to $\boldsymbol{n} = -\boldsymbol{c}_{k_0}$. This suggests, that an idea similar to the one in Section 4.1 can be used. We set

$$
\tilde{u}_{k_0}(n, \boldsymbol{j}) = \hat{u}_{k_0}(n, \boldsymbol{j}), \quad \boldsymbol{e}_{k_0} = s\boldsymbol{n} \tag{38}
$$

$$
\tilde{u}_k(n, \boldsymbol{j}) = \hat{u}_k(n, \boldsymbol{j} - \boldsymbol{n}), \quad \boldsymbol{e}_k \neq \boldsymbol{e}_{k_0} \tag{39}
$$

and prescribe $\tilde{\boldsymbol{u}}$ as Dirichlet condition on the outflow boundary. Observe that Equation (38) is practically an empty condition since the first equation in (10) follows from Equation (37). To enforce the Dirichlet condition, we again use the BFL method for *all* incoming directions

$$
f_i(n+1, \boldsymbol{j})
$$
$$
= f_{i^*}^c(n, \boldsymbol{j} + \boldsymbol{c}_i) + 6 f_i^* \tilde{\boldsymbol{u}}(n, \boldsymbol{j}) \cdot \boldsymbol{c}_i, \quad \boldsymbol{c}_i \neq \boldsymbol{n}. \tag{40}
$$

An asymptotic analysis reveals that Equations (37) and (40) approximate the do nothing condition (6) with at least first order accuracy.

5 Experiments and discussion

To evaluate the outflow boundary conditions, we set up two tests. One is to check how the conditions influence the inner flow relatively far away from the outflow. The other is to check whether the conditions let the fluid pass through the boundary so naturally as if there was no boundary.

To reach these aims, the benchmark problems described detailedly in Hanke (2004), Heywood et al. (1996) and Schäfer and Turek (1996) are employed. These papers also provide a number of reference values to verify the following results. The benchmark has also been used in Filippova and Hänel (1998) to test a Dirichlet boundary scheme for the lattice Boltzmann method. Figure 2 shows the primary configuration of the benchmark. Both model flows take place in an infinitely long 2D channel between two fixed solid walls parallel to the x-axis. The flow is at rest initially and driven by a constant velocity at the left end. A solid circular obstacle is placed near the channel entrance. The artificial outflow boundary is set at the right end. The disk has a slight downward offset to the channel axis with the same distance to inlet and bottom wall. The inflow condition is defined by

$$
U(0, y) = -4U_m y(y - H)/H^2, \quad V = 0. \tag{41}
$$

Here $H = 0.41\,\mathrm{m}$ is the height of channel. The diameter of the disk is $D = 0.1\,\mathrm{m}$. The blockage ratio D/H is fixed for all the numerical experiments. The fluid viscosity is $\nu = 10^{-3}\,\mathrm{m^2/s}$. The Reynolds number is defined by $Re = \bar{U}D/\nu$ with a mean velocity $\bar{U} = 2U_m/3$. The two test flows are distinguished by different values of U_m.

i $U_m = 0.3\,\mathrm{m/s}$ produces a Reynolds number $Re = 20$ and leads to a steady flow with a closed steady recirculation region consisting of two vortices behind the disk.

ii $U_m = 1.5\,\mathrm{m/s}$ yields a Reynolds number $Re = 100$ and renders an unsteady flow, behind the disk with a periodic vortex street.

In order to check how the outflow conditions influence the inner flow, some quantities around the disk are checked including the drag coefficient C_d, lift coefficient C_l and the pressure difference $\triangle P$ between the front and end point of the disk, i.e., $\triangle P = p(0.15, 0.2) - p(0.25, 0.2)$. The momentum-exchange method from Ladd (1994) is used to calculate these numbers. In Caiazzo and Junk (2007) the accuracy of this method is theoretically analysed.

In order to investigate all the methods carefully, we design the experiments in two series. One is fixing the grid size and setting different ratios between the channel length and width. The other is fixing the channel length/width ratio and changing the grid size.

In the lattice Boltzmann setup, the discrete velocity set is D2Q9, the collision operator is the BGK model with a single time relaxation parameter τ. The numerical

Figure 2 Configuration of 2D test cases
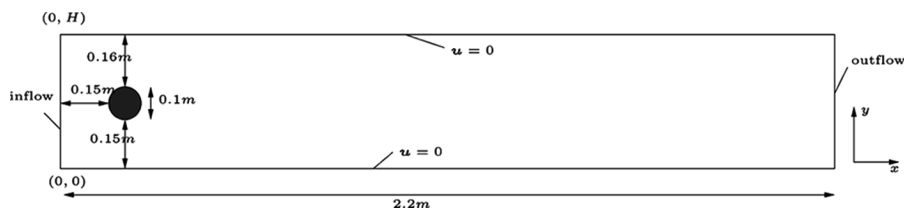
viscosity is $\nu = 1/Re$. Since at all inflow and rigid walls the boundary condition is Dirichlet type, either BFL from Bouzidi et al. (2001) or POP_1 from Junk and Yang (2005) is used. In case that BFL is applied, POP_1 is used for the opposite incoming directions at corner nodes. The grid nodes are located on the upper and bottom walls. The outflow condition is realised with the methods described in Section 4. At corner nodes where two types of boundary conditions meet, we have used the Dirichlet condition.

Stopping criterion

As criterion for stationary in our test case, we evaluate the approximate time derivative of the density $\hat{\rho}$. If the variation is sufficiently small

$$\max_{\boldsymbol{x_j} \in \Omega} |\hat{\rho}(n+1, \boldsymbol{x_j}) - \hat{\rho}(n, \boldsymbol{x_j})| < h^6, \qquad (42)$$

the numerical velocity and pressure fields are considered as approximations for the steady flow solutions.

5.1 Steady flow around a circular cylinder

Table 1 shows our calculations of drag coefficient (C_d), lift coefficient (C_l), and the pressure difference ($\triangle P$) for the steady flow. The 2nd and 3rd rows in the table provide the reference upper and lower bounds.

Table 1 Comparison results for steady flow around a disk. With respect to the size of the reference values, the results vary only a little. In particular, increasing the length of the channel has less influence on the results than refining the grid in the short channel. In other words, all outflow conditions simulate the longer channel reasonably well

	L/H	Grid	C_D	C_l	$\triangle P$
Lower			5.5700	0.0104	0.1172
Upper			5.5900	0.0110	0.1176
NBC	2	41×82	5.5792	0.0108	0.1194
	2	82×164	5.5795	0.0117	0.1171
	2	123×246	5.5816	0.0111	0.1174
	4	41×164	5.5798	0.01105	0.1194
ZNS	2	41×82	5.5662	0.0108	0.1192
	2	82×164	5.5838	0.0117	0.1172
	2	123×246	5.5713	0.01106	0.1172
	4	41×164	5.5808	0.0111	0.1195
DNT	2	41×82	5.5826	0.0111	0.1195
	2	82×164	5.5816	0.0117	0.1172
	2	123×246	5.5820	0.0111	0.1174
	4	41×164	5.5811	0.0111	0.1195

First let us observe the results in a short channel with fixed ratio $L/H = 2$ on three grids. It is found that finer grids render more accurate values in a relative short channel and agree well with the reference values. In addition, Table 1 also shows the results on a coarse grid with a large ratio $L/H = 4$. Obviously, enlarging L/H does not change the result considerably. This justifies the conclusion that all the outflow schemes approximate the real fluid movement

to some extent. Next, we investigate the behaviour when flow passes through the outflow. The values of velocity and pressure are compared along two cuts in the computational domain. The first cut line is through the center of the disk ($y = 0.20m$) and parallel to the wall. It is used to observe the velocity and pressure varying with the x-coordinate. The second cut line at $x = 2H$ is used to investigate the velocity and pressure variation vs. the y-coordinate at the outflow boundary. The grid is the finest one 123×246 ($L/H = 2$). We find that all the methods yield smooth solutions up to the outflow plane. ZNS and DNT lead to solutions close to each other and slightly different from the one produced by the NBC condition, which is illustrated by taking the horizontal velocity component as example in Figure 3.

Figure 3 Left: Plots of the horizontal velocity component vs. x along the line through the center of disk with 246 grid nodes along the x axis. Right: Plots of horizontal velocity component vs. y along the outflow with 123 grid nodes along the y axis. The symbols ∇, $+$ and $\circ$ stand for NBC, ZNS and DNT respectively
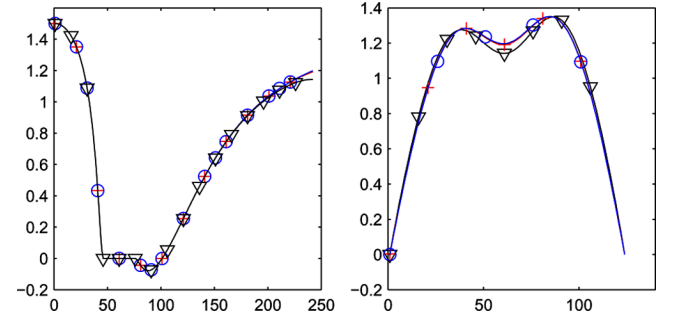

5.2 Unsteady flow around a circular cylinder

The Reynolds number for this unsteady flow is $Re = 100$. The numerical tests are carried out on the grids 82×164 ($L/H = 2$), 82×246 ($L/H = 3$), 82×410 ($L/H = 5$).

Figure 4 shows the quantities C_d, C_l and $\triangle P$ within 1000 time steps after the initial transient behaviour. The dash-dotted lines show the reference intervals from Schäfer and Turek (1996), which are the upper and lower bounds for the maximum drag coefficient, the maximum lift coefficient and the pressure difference on the cylinder after half a period from the time corresponding to the flow state with the maximum lift coefficient.

All the results show that the values are getting closer to the reference as the channel becomes longer, and ZNS and DNT produces much better results than NBC on all grids. Carefully comparing the size of these quantities, we find that ZNS and DNT yield C_d and $\triangle P$ for the short channel ($L/H = 2$) closer to the reference value than those given by NBC on a longer channel ($L/H = 3$). A similar comparison also holds for the channel $L/H = 3$ with ZNS or DNT and $L/H = 5$ with NBC. Comparatively, DNT influences the inner flow most weakly since the short channel ($L/H = 3$) has already produced nearly the same values as the one with large ratio $L/H = 5$.

Figure 4 The plots of C_d (left column), C_l (middle column) and $\triangle P$ (right column) for the unsteady flow with NBC (1st row), ZNS (2nd row) and DNT (3rd row). The dotted, dashed and solid lines stand for the result in the channel with $L/H = 2, 3, 5$ respectively. The dash-dotted line shows the reference intervals
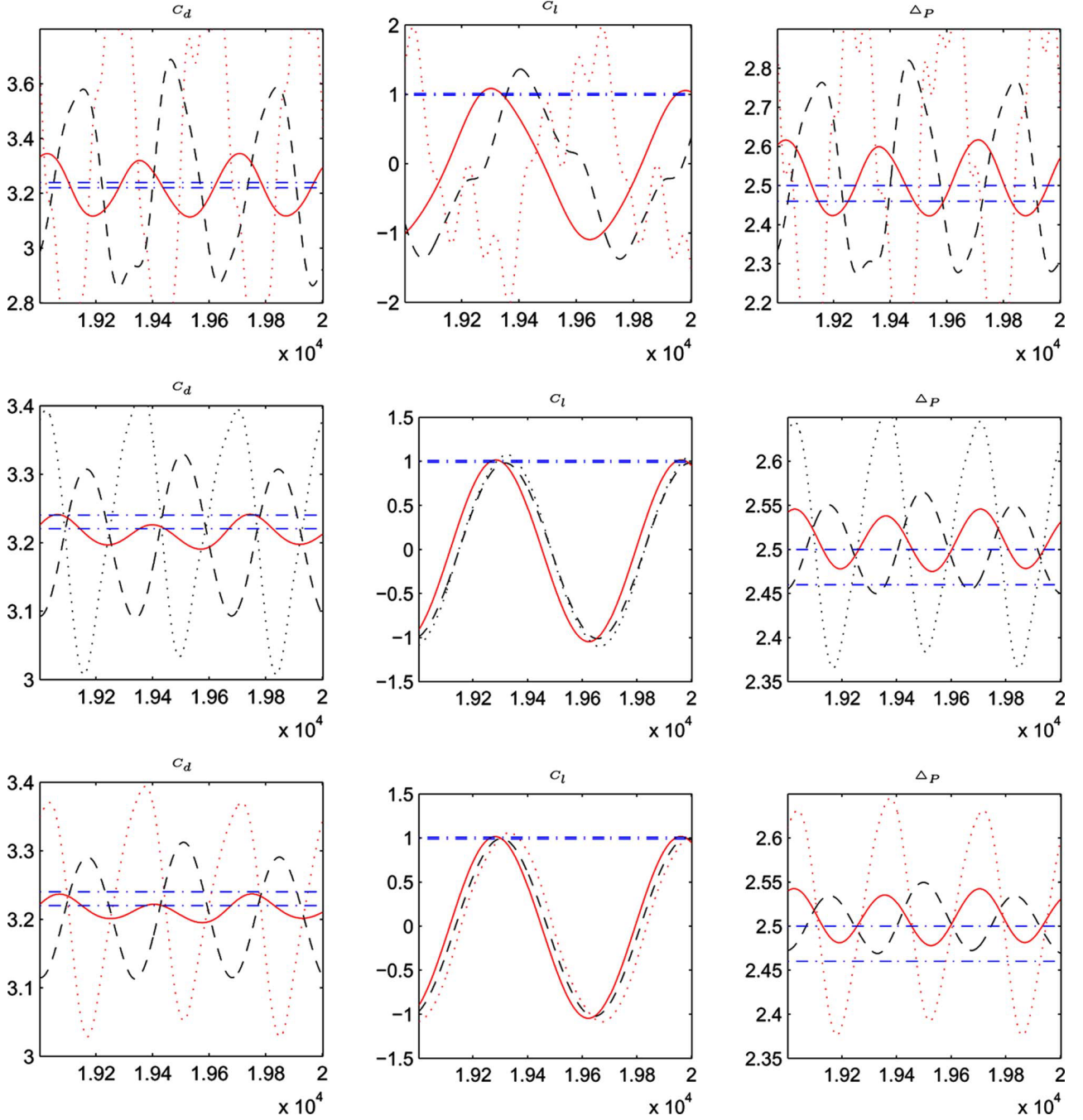

In addition, we know that there must be a vortex street behind the disk. Hence, the velocity and pressure variation vs. x should somehow be regular. We plot the velocity and pressure along the line through the center of the disk in Figure 5 for each outflow condition. From the plots for the NBC method, we see that the quantities behave differently behind the disk with respect to different L/H ratios. It demonstrates that the NBC outflow condition (16) has a strong impact on the inner flow. The methods ZNS and DNT yield more similar profiles with only a slight phase difference.

6 Conclusion

Frequently used Neumann type outflow conditions for FD and FEM simulations are constructed in this work for the lattice Boltzmann method. For each one we have proposed a first order accurate treatment. Using a stationary and a time-dependent channel flow, the features of these outflow schemes are investigated. For the stationary flow all three outflow schemes produce convincing results which are contained in the reference intervals described for this problem in Schäfer et al. (1998) and Schäfer

Figure 5 The plots of velocity and pressure (right) along the line through the center of the disk for the unsteady flow with NBC (1st row), ZNS (2nd row) and DNT (3rd row). The symbols $+$, $\circ$ and ∇ stand for the results in the channel with $L/H = 2, 3, 5$ respectively
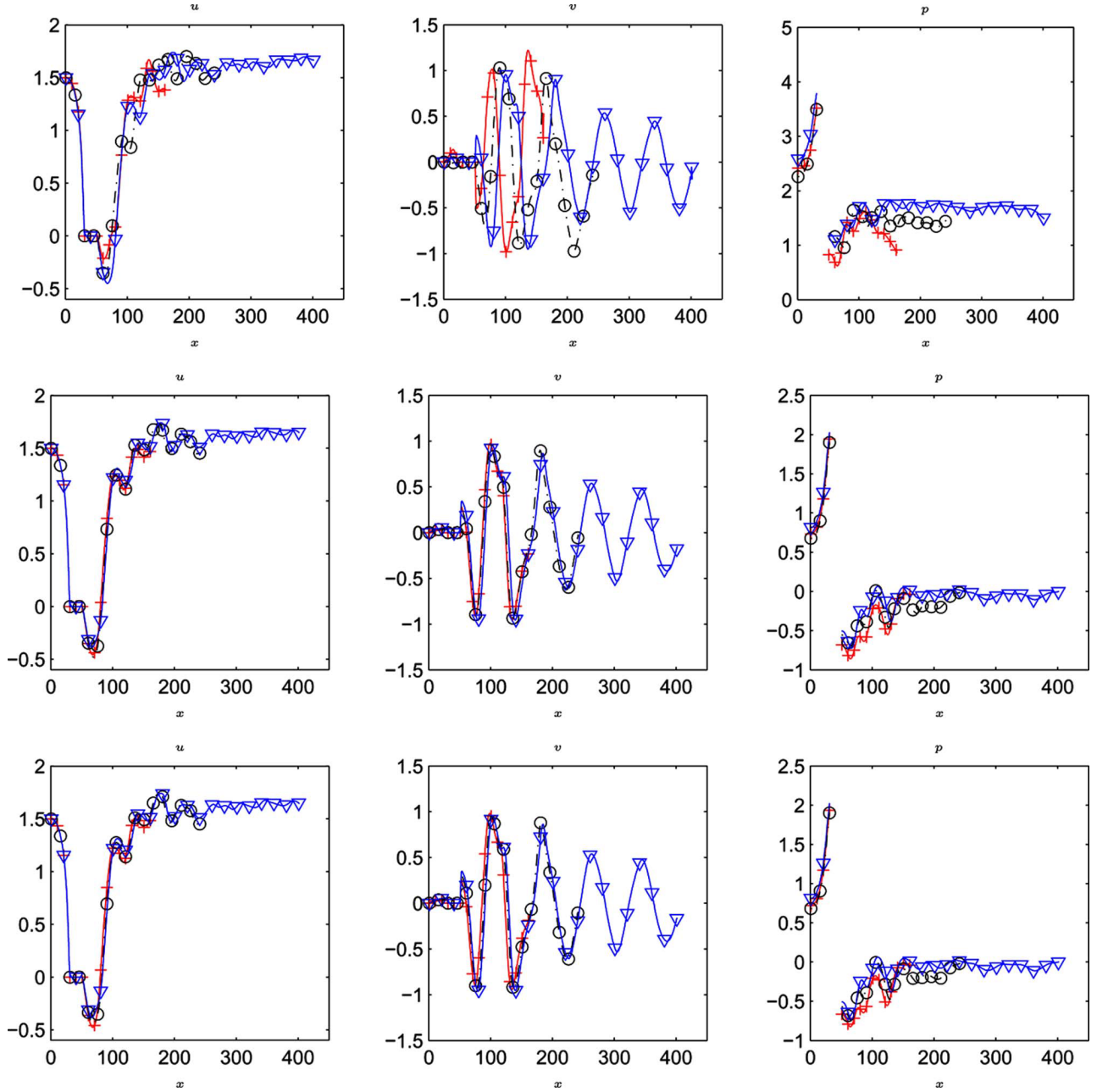
and Turek (1996), provided the grid is fine enough. In the nonstationary case, the zero Neumann scheme (16) destroys the vortex close to the outflow, the zero-normal-stress scheme (24), (30), (31) behaves better, and the do-nothing-scheme (37), (40) renders a slightly bigger effect on the inner flow. However, compared with the results in Filippova and Hänel (1998), Schäfer et al. (1998) and Schäfer and Turek (1996), our results are competitive. A generalisation of the methods to more general geometries is currently investigated.

Acknowledgment

References

Abbassi, H., Turki, S. and Ben Nasrallah, S. (2002) 'Channel flow past bluff-body: outlet boundary condition, vortex shedding and effects of buoyancy', *Computational Mechanics*, Vol. 28, pp.10–16.

Benzi, R., Succi, S. and Vergassola, M. (1992) 'The lattice-Boltzmann equation: Theory and applications', *Phys. Rep.*, Vol. 222, pp.145–197.

Bhatnagar, P., Gross, E. and Krook, M. (1954) 'A model for collision processes in gases i: small amplitude processes in charged and neutral one-component system', *Phys. Rev.*, Vol. 94, pp.511–525.

Bouzidi, M., Firdaouss, M. and Lallemand, P. (2001) 'Momentum transfer of a Boltzmann-lattice fluid with boundaries', *Phys. Fluids*, Vol. 13, No. 11, pp.3452–3459.

Caiazzo, A. and Junk, M. (2007) 'Boundary forces in lattice Boltzmann: analysis of momentum exchange algorithm', *Computers and Mathematics with Applications*, doi:10.1016/j.camwa.2007.08.004.

Chen, S. and Doolen, G.D. (1998) 'Lattice Boltzmann method for fluid flows', *Annu. Rev. Fluid Mech.*, Vol. 30, pp.329–364.

Chen, H., Chen, S. and Matthaeus, W.H. (1992) 'Recovery of the Navier-stokes equations using a lattice-gas Boltzmann method', *Phys. Rev. A*, Vol. 45, pp.R5339–5342.

Chen, H., Chen, S., Martinez, D. and Matthaeus, W.H. (1991) 'Lattice-gas Boltzmann model for simulation of magnetohydrodynamics', *Phys. Rev. L*, Vol. 67, p.3776.

Chikatamarla, S.S., Ansumali, S. and Karlin, I.V. (2006) 'Grad's approximation for missing data in lattice Boltzmann simulations', *Europhysics Letters*, Vol. 74, No. 2, pp.215–221.

d'Humières, D. (1992) 'Generalized lattice-Boltzmann equations. AIAA Rarefied gas dynamics: theory and simulations', *Progress in Astronautics and Aeronautics*, Vol. 59, pp.450–548.

d'Humières, D., Ginzbourg, I., Krafczyk, M., Lallemand, P. and Luo, L-S. (2002) 'Multiple-relaxation-time lattice Boltzmann models in three dimensions', *Phil. Trans. R. Soc. Lond. A*, Vol. 360, pp.437–451.

Filippova, O. and Hänel, D. (1998) 'Grid refinement for lattice-BGK models', *J. Comp. Phys.*, Vol. 147, pp.219–228.

Frisch, U., d'Humières, D., Hasslacher, B., Lallemand, P., Pomeau, Y. and Rivet, J.P. (1987) 'Lattice gas hydrodynamics in two and three dimensions', *Complex Sys.*, Vol. 1, pp.649–707.

Ginzburg, I. and Steiner, K. (2003) 'Lattice Boltzmann model for free-surface flow and its application to filling process in casting', *Journal of Computational Physics*, Vol. 185, No. 1, pp.61–99.

Hanke, M. (2004) *Benchmarking FEMLAB 3.0a: Laminar Flows in 2d*, Royal Institute of Technology, Report No. 2004:01, 01, 2004.

He, X. and Luo, L-S. (1997a) 'A priori derivation of the lattice Boltzmann equation', *Phys. Rev. E*, Vol. 55, pp.6333–6336.

He, X. and Luo, L-S. (1997b) 'Theory of the lattice Boltzmann method: from the Boltzmann equation to the lattice Boltzmann equation', *Phys. Rev. E*, Vol. 56, pp.6811–6817.

Heywood, J., Rannacher, R. and Turek, S. (1996) 'Artificial boundaries and flux and pressure conditions for the incompressible Navier-Stokes equations', *Int. J. Numer. Meth. Fluids*, Vol. 22, pp.325–352.

Junk, M., Klar, A. and Luo, L-S. (2005) 'Asymptotic analysis of the lattice Boltzmann equation', *J. Comp. Phys.*, Vol. 210, pp.676–704.

Junk, M. and Yang, Z. (2005) 'Asymptotic analysis of lattice Boltzmann boundary conditions', *J. Stat. Phys.*, Vol. 121, pp.3–35.

Ladd, A.J.C. (1994) 'Numerical simulations of particular suspensions via a discretized Boltzmann equation', *J. Fluid Mech.*, Vol. 271, pp.285–339.

Lamura, A., Gompper, G., Ihle, T. and Kroll, D.M. (2001) 'Multi-particle collision dynamics: flow around a circular and a square cylinder', *Europhysics Letters*, Vol. 56, No. 3, pp.319–325.

Mazya, V. and Rossmann, J. (2006) 'Mixed boundary value problems for the Navier-Stokes system in polyhedral domains', preprint in *Math. Meth. Appl. Sci.*, arXiv: math-ph/0602054v1.

McNamara, G.R. and Zanetti, G. (1988) 'Use of Boltzmann equation to simulate lattice-gas automata', *Phys. Rev. L*, Vol. 61, p.2332.

Mei, R., Luo, L-S. and Shyy, W. (1999) 'An accurate curved boundary treatment in the lattice Boltzmann method', *J. Comp. Phys.*, Vol. 155, pp.307–330.

Ol'shanskii, M.A. and Staroverov, V.M. (2000) 'On simulation of outflow boundary conditions in finite difference calculations for incompressible fluid', *Int. J. Numer. Meth. Fluids*, Vol. 33, pp.499–534.

Qian, Y., d'Humières, D. and Lallemand, P. (1992) 'Lattice BGK models for Navier-Stokes equation', Europhys. *Lett.*, Vol. 17, pp.479–484.

Schäfer, M., Rannacher, R. and Turek, S. (1998) 'Evaluation of a CFD benchmark for laminar flows', in Bock, H.G., Kuznetsov, Y.A., Glowinski, R., Periaux, J. and Rannacher, R. (Eds.): *ENUMATH97 Proceedings of the 2nd European Conference on Numerical Mathematics and Advanced Applications*, World Science Publishing, Singapore, pp.549–563.

Schäfer, M. and Turek, S. (1996) 'Benchmark computations of laminar flow around a cylinder', in Hirschel, E.H. (Ed.): *Flow Simulation with High-performance Computers II, Vol. 52 of Notes on Numerical Fluid Dynamics*, Vieweg, pp.547–566.

Yu, D., Mei, R. and Shyy, W. (2005) 'Improved treatment of the open boundary in the method of lattice Boltzmann equation', *Progress in Computational Fluid Dynamics*, Vol. 5, Nos. 1–2, pp.1–11.